© 2014. Published by The Company of Biologists Ltd | Development (2014) 141, 3072-3083 doi:10.1242/dev.101972

RESEARCH ARTICLE

Loss of focal adhesions in glia disrupts both glial and photoreceptor axon migration in the *Drosophila* visual system

Xiaojun Xie, Mary Gilbert, Lindsay Petley-Ragan and Vanessa J. Auld*

ABSTRACT

Many aspects of glial development are regulated by extracellular signals, including those from the extracellular matrix (ECM). Signals from the ECM are received by cell surface receptors, including the integrin family. Previously, we have shown that *Drosophila* integrins form adhesion complexes with Integrin-linked kinase and talin in the peripheral nerve glia and have conserved roles in glial sheath formation. However, integrin function in other aspects of glial development is unclear. The *Drosophila* eye imaginal disc (ED) and optic stalk (OS) complex is an excellent model with which to study glial migration, differentiation and glia-neuron interactions. We studied the roles of the integrin complexes in these glial developmental processes during OS/eye development. The common beta subunit βPS and two alpha subunits, αPS2 and αPS3, are located in puncta at both glia-glia and glia-ECM interfaces. Depletion of βPS integrin and talin by RNAi impaired the migration and distribution of glia within the OS resulting in morphological defects. Reduction of integrin or talin in the glia also disrupted photoreceptor axon outgrowth leading to axon stalling in the OS and ED. The neuronal defects were correlated with a disruption of the carpet glia tube paired with invasion of glia into the core of the OS and the formation of a glial cap. Our results suggest that integrin-mediated extracellular signals are important for multiple aspects of glial development and non-autonomously affect axonal migration during *Drosophila* eye development.

KEY WORDS: Integrin, Talin, Glia, Optic stalk, Eye, Axon stalling

INTRODUCTION

Glia provide neurons with metabolic and structural support as well as playing a direct role in guiding neuronal development (Eroglu and Barres, 2010; Freeman and Doherty, 2006; Parker and Auld, 2006). Many aspects of glial development are intimately tied to neuron-generated signals through either direct cell-cell contact or secreted factors (Newbern and Birchmeier, 2010). Other than neurons, regulatory signals are also provided to glia by the extracellular matrix (ECM) and adjacent glia. Integrins are a key family of ECM receptors important for both neuronal and glial development (Clegg et al., 2003; Milner and Campbell, 2002). Integrins are heterodimeric transmembrane proteins, composed of one alpha and one beta subunit, that control a wide range of cellular responses including adhesion, migration and differentiation (Takada et al., 2007). Integrins are components of focal adhesions, which also include proteins such as talin, vinculin, tensin, paxillin and Focal adhesion kinase (FAK) (Brakebusch and Fässler, 2003). Talin, a key component of focal adhesions, binds the cytoplasmic tail of β-integrins, linking them to the actin cytoskeleton and mediating integrin activation (Critchley, 2000; Critchley et al., 1999).

During glial development, integrins are necessary for the radial sorting of axons and for subsequent myelination by oligodendrocytes and Schwann cells (Barros et al., 2009; Benninger et al., 2007; Camara et al., 2009; Feltri et al., 2002; Lee et al., 2006; Nodari et al., 2007; Yu et al., 2009). Similarly, loss of FAK or Integrin-linked kinase (ILK) mimics the phenotype of β1-integrin-deficient glia of both the PNS and CNS (Grove et al., 2007; Pereira et al., 2009). However, the role that integrins play earlier in glial development or in non-myelinating glia is unclear and the role of talin in glial development has yet to be determined.

The diversity and combination of multiple vertebrate integrin subunits (Milner and Campbell, 2002; Previtali et al., 2001) complicates the investigation of their function. *Drosophila* is advantageous for such studies as it has a simple family of integrin subunits consisting of five alpha and two beta subunits (Brown et al., 2000). Furthermore, the eye and optic stalk is an excellent model for studying glial development and, in particular, permits detailed analysis of glia-axon, glia-glial and glia-ECM interactions (Silies et al., 2010). The late larval optic stalk (OS) contains three distinct glial layers (Fig. 1A): the outermost perineurial glia (PG), the intermediate carpet glia (CG) and the internal wrapping glia (WG). Collectively, they ensheath the photoreceptor axons extending from the eye disc (ED) through the OS into the optic lobe (Silies et al., 2007; Tayler and Garrity, 2003). In early larval stages the two CG, which are specialized subperineurial glia (SPG), form a tubular glial structure encircled by a monolayer of PG. Photoreceptor axons from the developing ED migrate within this tube in the late third instar to targets in the proximal optic lobe (Silies et al., 2007). Starting in the mid-third instar, both CG and PG migrate from the OS into the ED – the CG along the basal surface of the disc epithelia and the PG between the CG and the basal ECM (Silies et al., 2007). At the distal end of the CG border, neuron-derived signals trigger differentiation of the migrating PG into WG (Franzdottir et al., 2009). Differentiated WG reverse their direction of migration and travel proximally through the OS, contacting and ensheathing the photoreceptor axons. Throughout these events glia make extensive contact with both the ECM and other glia, but the role of focal adhesion complexes in these processes is unknown.

Integrin-associated FAK has been suggested to genetically interact with βPS integrin and control OS morphogenesis (Murakami et al., 2007). Whether integrins and other adhesion complex components are necessary for glia migration and development in the eye has yet to be determined. Here we show that *Drosophila* integrin- and focal adhesion-mediated glia-ECM and glia-glia interactions are necessary for retinal glia development. Specifically, the loss of βPS integrin or talin compromises glial migration into the ED and leads to changes in

Department of Zoology, Cell and Developmental Biology, Life Sciences Institute, University of British Columbia, 2350 Health Sciences Mall, Vancouver, BC, Canada V6T 1Z3.

*Author for correspondence (auld@zoology.ubc.ca)

Received 2 August 2013; Accepted 2 June 2014

Development (2014) 141, 3072-3083 doi:10.1242/dev.101972

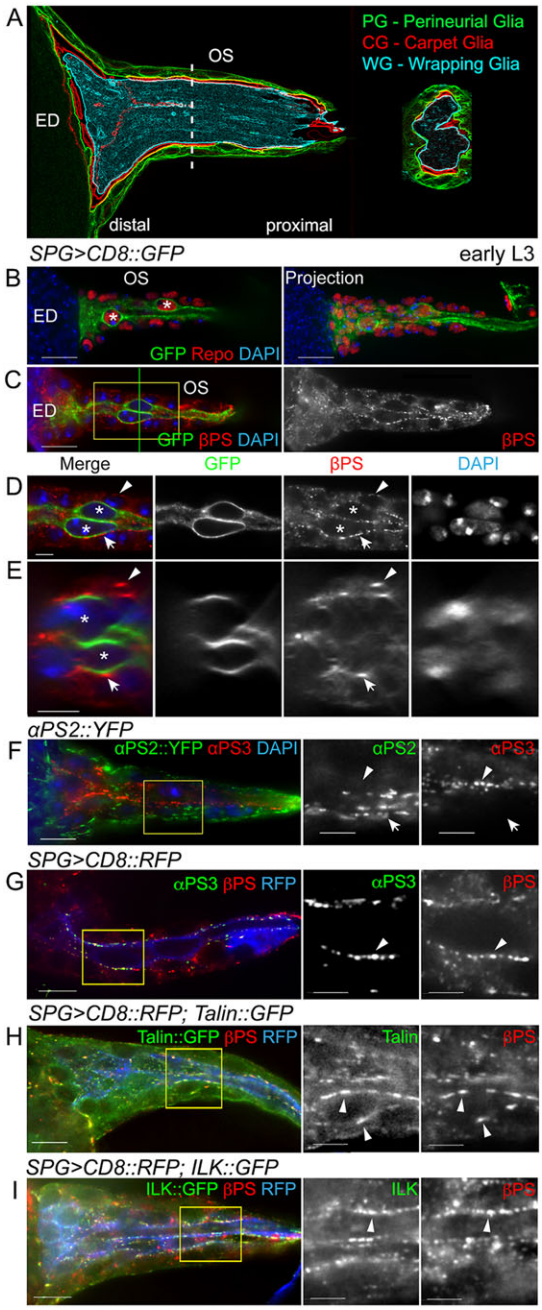

Fig. 1. Integrin subunit and talin expression in the eye disc and optic stalk. (A) The three glial layers of the optic stalk (OS): the perineurial glia (PG, green), carpet glia (CG, red) and wrapping glia (WG, cyan). The dashed line indicates the plane of section shown to the right. ED, eye disc. (B-I) Focal adhesion components in the OS of early third instar larvae. (B) Repo immunolabeling (red) of all glial nuclei. The two CG were labeled by *SPG>CD8::GFP* (green) and asterisks mark the larger CG nuclei. (C-E) βPS labeling and *SPG>CD8::GFP* (green) labeled CG (asterisks). D is a digital expansion of the boxed region in C. The green line in C shows the position of the orthogonal sections in E. βPS integrin forms puncta located at the PG-ECM (arrowheads) and PG-CG (arrows) interface. (F) αPS2 (green) and αPS3 (red) integrin subunits. αPS2::YFP was primarily located in the outer PG (arrow), whereas αPS3 immunolabeling was predominant in the central CG (arrowhead). (G) αPS3 (green) and βPS (red) integrin subunits. αPS3 and βPS were colocalized in puncta in the central CG (arrowhead). (H,I) Colocalization of talin::GFP (G, green) or ILK::GFP (H, green) with βPS immunolabeling (red, arrowheads). All panels are single 0.2 μm *z*-sections except for the projection in B. Boxed regions in F-I are digitally expanded and shown to the right. Scale bars: 10 μm in B,C and in F-I (left); 5 μm in D,E and in F-I (middle and right).

glial organization within the OS paired with axon stalling and a failure of axons to enter the brain lobe.

RESULTS

Integrins and focal adhesion proteins are expressed in the glia of the larval optic stalk

To determine the integrin expression pattern in the glia of the OS and ED, we used an antibody to the single essential beta subunit in *Drosophila*, βPS [also known as Myospheroid (Mys)]. We detected βPS in OS glia in early third instar larvae (Fig. 1C-E). βPS was located in puncta, similar to those observed in the peripheral nerve (Xie and Auld, 2011), that were located at the interface of the PG layer and the ECM, the PG-CG interface, and between the two CG (Fig. 1D,E).

Drosophila melanogaster has five α-integrin subunits, of which only αPS1-3 (also known as Multiple edematous wings, Inflated and Scab, respectively) have vertebrate counterparts (Takada et al., 2007). Using immunolabeling and endogenously tagged proteins, we found that αPS2 and αPS3, but not αPS1, were present in the ED and OS. In early L3, αPS3 was predominantly at the PG-CG interface (Fig. 1F,G) in the OS, and αPS2 was primarily between the PG and ECM (Fig. 1F). We assayed for the presence of the focal adhesion markers talin (Rhea – FlyBase) and ILK, both endogenously tagged with GFP, and found βPS colocalized with both (Fig. 1H,I). These focal adhesions persist and, in wandering larvae, integrin colocalized with talin- and ILK-labeled puncta, primarily on the outer surface of the PG contacting the ECM (supplementary material Fig. S1). Some integrin immunolabeling was observed in the WG associated with the photoreceptor axons in the OS of wandering stage larvae (supplementary material Fig. S1). These results suggest that βPS integrin together with specific alpha subunits are components of focal adhesions positioned to mediate glia-ECM, glia-glia or glia-neuron interactions.

βPS integrin and talin are required for glial organization and migration in the OS

βPS genetically interacts with *Fak56D* and regulates PG distribution along the OS (Murakami et al., 2007). However, it was unclear whether integrins are involved in other aspects of glial development such as migration and differentiation, and whether glial integrins affect photoreceptor axon outgrowth. As loss-of-function mutants in the *βPS* (*mys*) gene are embryonic lethal, we used RNAi to determine integrin function in OS and ED development in third instar larvae.

To analyze the roles of integrin in glia at larval stages, we used the pan-glial driver repo-GAL4 to drive the expression of RNAi constructs previously shown to knock down βPS and talin (Perkins et al., 2010; Xie and Auld, 2011). When repo-GAL4 drove the respective RNAi (*repo>βPS-RNAi* or *repo>talin-RNAi*), βPS or talin immunolabeling was absent in the OS glia, whereas the integrin complexes within the ED epithelia remained intact (supplementary material Fig. S2).

In both *repo>βPS-RNAi* and *repo>talin-RNAi* we observed morphological changes in the OS as the distal end became thicker compared with controls. This phenotype was observed in both early (supplementary material Fig. S2) and wandering third instar (Fig. 2) larvae and was consistently observed in two independent RNAi constructs for each gene. Two glial aberrations were observed corresponding to the morphological changes in the OS. First, PG nuclei aggregated in the distal half of the thickened OS (Fig. 2B,C,D,F), in contrast to the normally uniform distribution (Fig. 2A,E). The corresponding proximal end was thinner and contained the CD8::GFP-labeled membrane of the CG projection

Development (2014) 141, 3072-3083 doi:10.1242/dev.101972

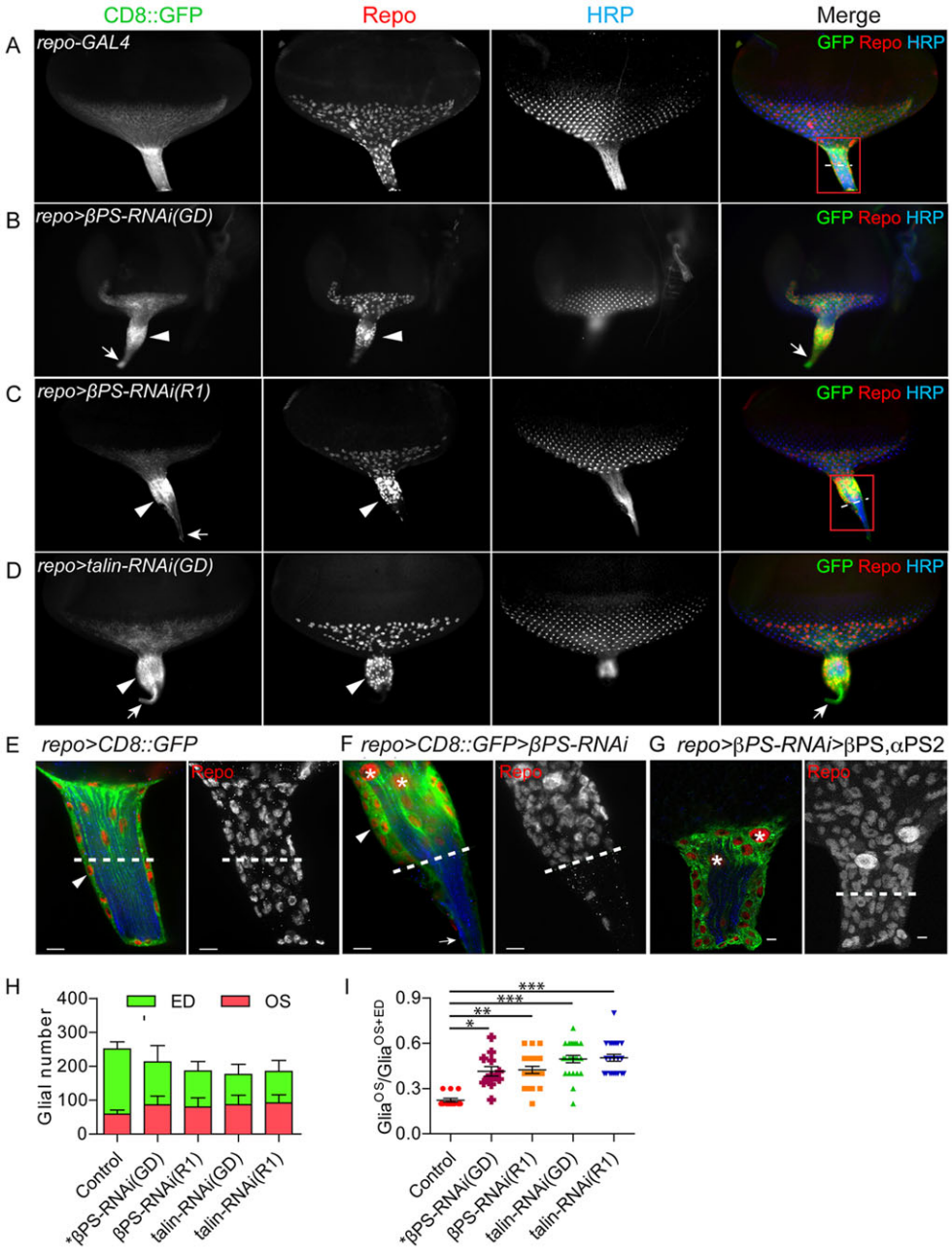

Fig. 2. Alterations in OS morphology and glial migration upon downregulation of integrin and talin. RNAi lines were expressed in all glia using repo-GAL4 with UAS-CD8::GFP (green) to label glial membranes. Glial nuclei and photoreceptor cells were immunolabeled with antibodies to Repo (red) and HRP (blue). (A-D) Compared with control (A), *repo>βPS-RNAi* and *repo>talin-RNAi* had thicker OSs (B-D, arrowheads). Glial nuclei aggregated at the anterior half of the OS and CD8::GFP-labeled glial membranes extended to the thinner posterior end of the OS (B-D, arrows). (E-G) High-magnification images of control, βPS-RNAi OS and rescued βPS-RNAi OS. (E,F) The boxed regions in A and C are shown at high magnification, with single 0.2 μm sections (left) and projections of the entire *z*-stack for Repo immunolabeling (right). (F) The PG are multilayered (arrowhead) with a fine projection of CD8::GFP-labeled CG at the proximal end (arrow). Dashed lines show the midpoint of each OS. (G) *repo>CD8::GFP>βPS-RNAi(GD)* with co-expression of βPS and αPS2, which rescued the glial morphological defects. Asterisks highlight the two CG nuclei. Scale bars: 5 μm. (H) Quantification of glial number separately in the ED and OS in *repo>Dicer2* (control, *n*=13), *repo>βPS-RNAi(GD)* (*n*=12), *repo>βPS-RNAi(R1)* (*n*=21), *repo>talin-RNAi(GD)* (*n*=23) and *repo>talin-RNAi(R1)* (*n*=22). Glial number was scored by Repo immunolabeling at wandering L3 with 11-15 rows of ommatidia. (I) The ratio of glia in the OS ($Glia^{OS}$) compared with glia in the OS plus ED ($Glia^{OS+ED}$). Larger ratios indicate more glia in the OS. Lines indicate the mean ratio and s.e.m. **P*<0.05, ***P*<0.01, ****P*<0.001 (one-way ANOVA with Dunn's multiple comparison test).

along the full length of the OS. Second, the PG formed aggregates instead of the normal monolayer, resulting in a greater OS diameter (Fig. 2F). These OS phenotypes were rescued by co-expressing a βPS transgene with the βPS-RNAi in glia (Fig. 2G), along with the αPS2 subunit to block the dominant-negative effects of βPS alone (Han et al., 2012).

We observed more glia located in the RNAi-treated OS than in controls, and measured the average number of glia in control and RNAi-expressing animals with 11-15 rows of ommatidia in the ED (Fig. 2H). On average, the RNAi-treated OS contained 36-56% more glia and the RNAi-treated ED 33-54% fewer glia than controls. To better show the relative distribution of glia between the ED and OS, the ratio of glia in the OS was compared with the entire population in the OS plus the ED (Fig. 2I). This ratio significantly increased from 0.22 in controls to 0.41-0.50 in RNAi-expressing larvae. Our data suggest that βPS integrin and talin play a role in PG migration from the OS into the ED and that the changes in glial distribution lead to a thicker OS.

In the normal OS, PG are physically separated from the internal photoreceptor axons and the WG by the glial tube formed by the CG (Franzdottir et al., 2009). In the absence of a specific membrane marker for the CG, we assayed the integrity of the CG sheath and changes in CG morphology using the transmembrane protein Neurexin IV endogenously tagged with GFP (NrxIV::GFP). NrxIV is a core component of septate junctions (SJs) and is specifically expressed in the SPG to generate the blood-brain barrier (Baumgartner et al., 1996; Silies et al., 2007; Stork et al., 2008). In the OS of normal early third instar larvae (*n*=6/7), NrxIV::GFP localized to two condensed lines between the two CG (Fig. 3A,B) and extended the entire length of the OS to the ED, where an NrxIV::GFP-positive end-foot was seen (Fig. 3B). The majority of *repo>βPS-RNAi(R1)* OSs (*n*=6/8) displayed a disorganized

Development (2014) 141, 3072-3083 doi:10.1242/dev.101972

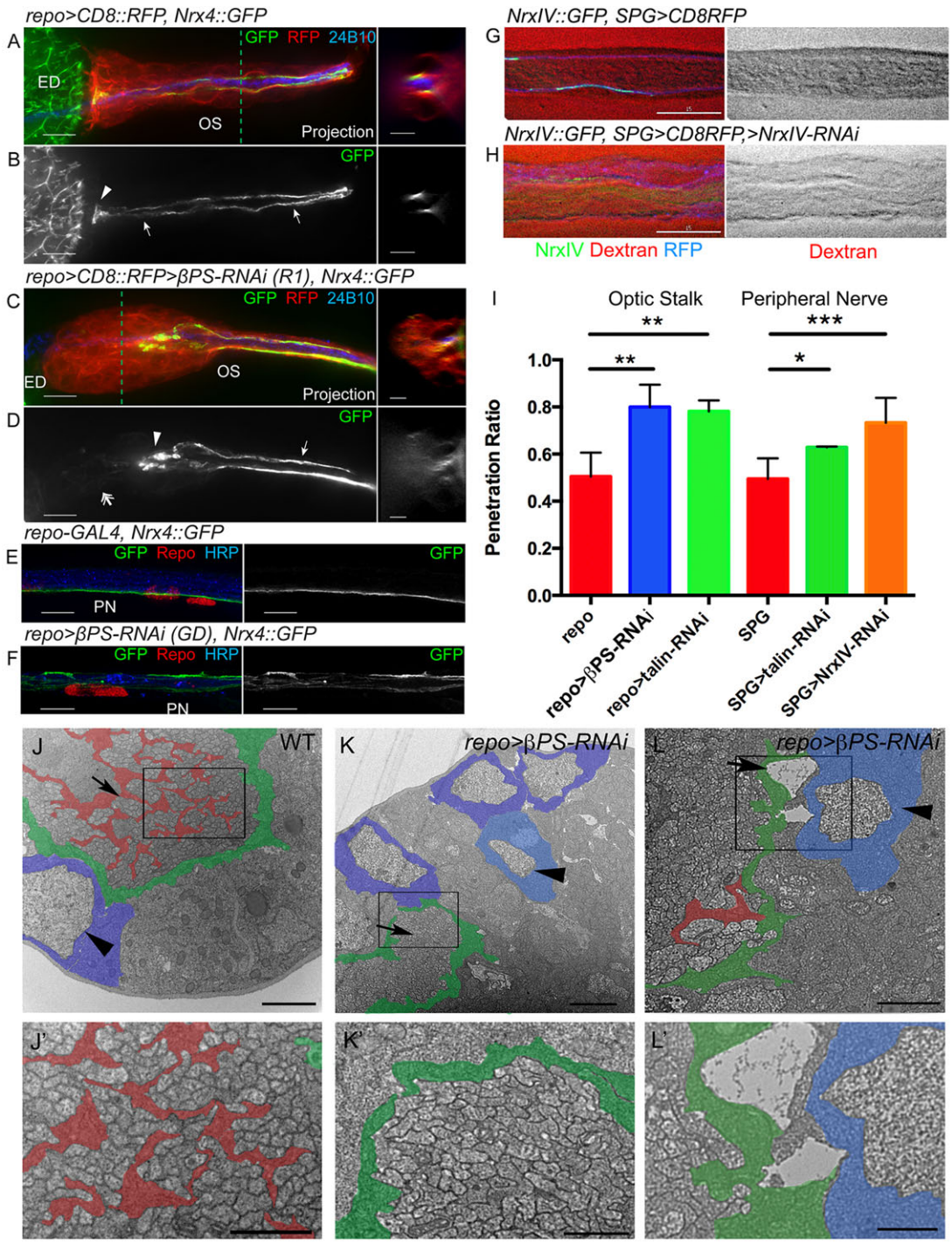

Fig. 3. CG and PG defects are observed upon integrin knockdown. (A-D) The morphology of the CG was assayed using NrxIV::GFP in early third instar larvae. (Left) *z*-stack projections; (right) orthogonal sections at the dashed lines. repo>CD8::RFP (red) marked glial membranes and 24B10 immunolabeling (blue) labeled Bolwig's nerve. In controls (A,B), NrxIV::GFP labeled the two septate junctions (SJs; arrows) formed between the CG along the OS and the end-feet at the distal end (arrowhead). In *repo>βPS-RNAi(R1)* (C,D), NrxIV::GFP stopped in the middle of the OS (arrowhead) and was disorganized or diffuse at the distal end (double arrow). The CG still formed a tube-like structure in the proximal half of the OS and NrxIV::GFP condensed into two normal lines (D, arrow). (E,F) NrxIV::GFP was used to label the SPG in wandering L3 peripheral nerves (PN). Repo and HRP immunolabeling of glial nuclei and axons, respectively. In controls (E), NrxIV::GFP was concentrated in a single line marking the SJs along the SPG. NrxIV::GFP disruption was observed in the *repo>βPS-RNAi(GD)* peripheral nerve (F). (G-I) Dye permeability assays were conducted to determine if CG ensheathment and blood-nerve barrier formation were disrupted. Examples of control (G) and NrxIV-RNAi (H) are shown to illustrate the full extent of dye exclusion (G) and of dye penetration (H). (I) The ratios of dye penetration for the peripheral nerve and OS are shown with s.d. indicated. Each experimental sample exhibited significantly greater dye penetration than the control. Dye penetration between the two control genotypes was not significantly different. **P*<0.05, ***P*<0.01, ****P*<0.001 (unpaired *t*-test with Welch's correction). (J-L′) TEM analysis of late third instar OSs from wild-type control (J), and *repo>βPS-RNAi(GD)* (K,L). The boxed areas are shown at higher magnification in J′-L′. False coloring indicates the WG (red), PG (blue) and CG (green). (J) In controls, WG ensheath photoreceptor axon bundles (arrow) and PG form a monolayer (arrowhead). (K,L) Photoreceptor axons were not bundled in the βPS-RNAi OS (K, arrow) and breaks between the glial layers were observed (L, arrow). Ectopic PG (light blue, arrowheads) were found within the OS. Scale bars: 10 μm in A-F (left) and G,H; 5 μm in A-D (right); 1 μm in J-L; 2 μm in J′-L′.

Development (2014) 141, 3072-3083 doi:10.1242/dev.101972

NrxIV::GFP pattern in which NrxIV::GFP failed to form condensed lines at the distal end of the OS and terminated prematurely in the middle of the OS (Fig. 3D). The NrxIV::GFP labeling often appeared diffuse or bunched (Fig. 3C,D), suggesting that the CG processes were retracted or disrupted. Interestingly, the NrxIV::GFP distribution appeared to be normal in the proximal half of the OS (Fig. 3D). The distribution of NrxIV::GFP in βPS-depleted larvae was not restricted to the OS; NrxIV::GFP disorganization was also seen in the peripheral nerves (Fig. 3F), suggesting that βPS integrin is required globally by *Drosophila* glia to maintain the sheath and SJ formation. Similar results were observed with *repo>talin-RNAi* in the OS glia (supplementary material Fig. S2). These data suggest that the loss of focal adhesions results in a disruption of SJ formation and/or maintenance.

We developed a dye permeation assay to test the integrity of the SJ and the blood-nerve barrier. To confirm the feasibility of this assay we first tested peripheral nerves of the third instar larvae (Fig. 3G,H). In control larvae (SPG-GAL4, *n*=19), Alexa 647 conjugated to 10 kDa dextran was unable to penetrate the peripheral nerve (Fig. 3G). By contrast, knockdown of NrxIV in the SPG (*SPG>NrxIV-RNAi*, *n*=4) disrupted the blood-nerve barrier, and dye diffused freely into the peripheral nerve (Fig. 3H). The degree of dye penetration was quantified by comparing the intensity of the dye within the nerve to a similar area outside (Fig. 3I). We then tested the effect of knockdown of βPS and talin and found a significant difference in dye penetration in both the peripheral nerves of *SPG>talin-RNAi* (*n*=4) and OS of *repo>βPS-RNAi* (*n*=9) or *repo>talin-RNAi* (*n*=15) compared with control (*repo-GAL4*, *n*=19) (Fig. 3I; supplementary material Fig. S3). These results support the observation that CG morphology is disrupted when focal adhesions are absent.

To analyze these glial morphology changes at the ultrastructural level, we carried out TEM analysis of the *repo>βPS-RNAi* OS compared with controls (Fig. 3J-L). In wild type (Fig. 3J), the WG ensheath the bundles of photoreceptor axons and the PG form a monolayer around the OS as previously described (Silies et al., 2007). In *repo>βPS-RNAi* larvae, the photoreceptor axons bundles were not separated (Fig. 3K). Multiple PG were stacked between the

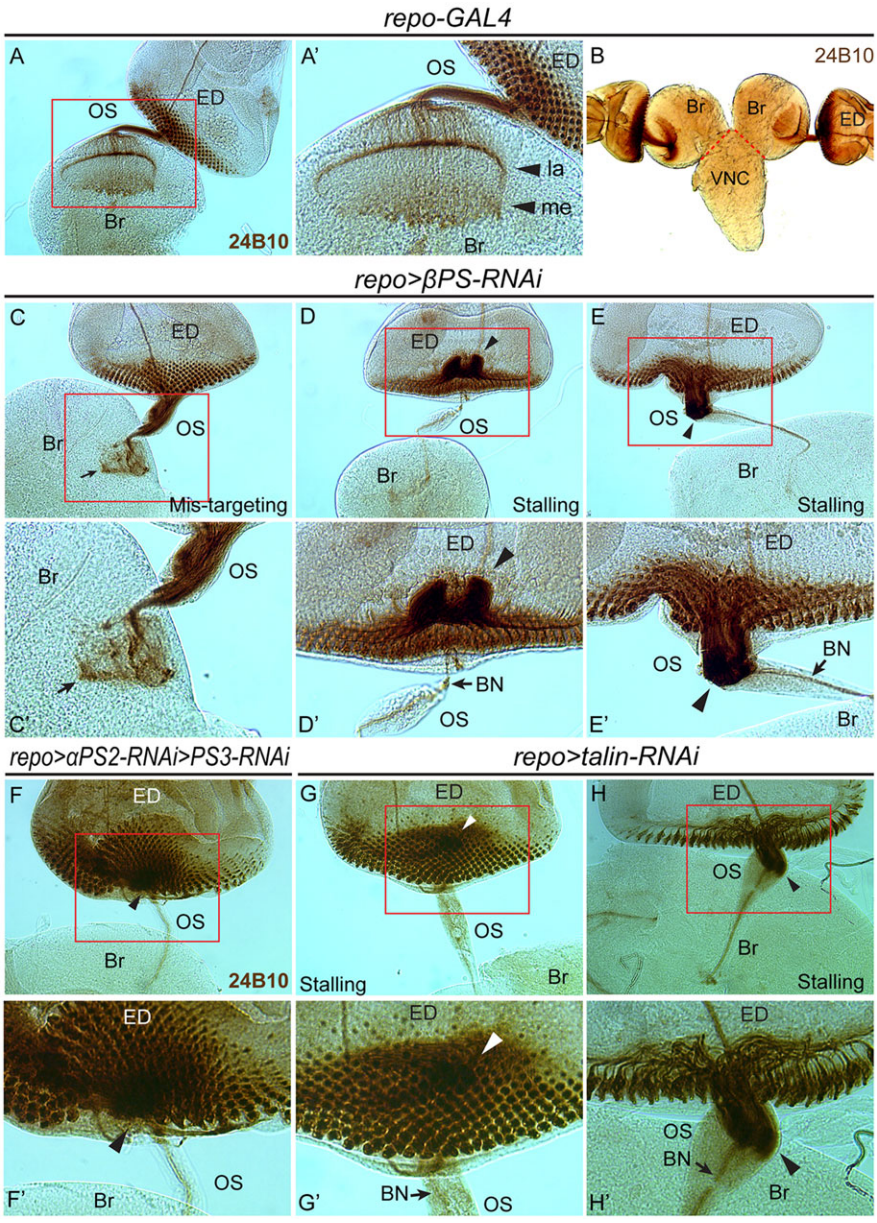

Fig. 4. Photoreceptor axon migration defects observed with focal adhesion loss in glia. Photoreceptors were immunolabeled with anti-Chaoptin antibody (mAb 24B10). (A-B) In control larvae, photoreceptor axons exited the ED, passed through the OS and terminated in the lamina (la) and medulla (me) (A′) in the brain lobe (Br). VNC, ventral nerve cord. (C-E′) In *repo>βPS-RNAi* larvae, the photoreceptor axons exhibited a disorganized pattern in the brain lobe (C,C′, arrow), failed to exit the ED (D,D′, arrowheads) or stalled in the OS (E,E′, arrowheads). BN, Bolwig's nerve. (F-H′) Axon stalling phenotypes were also observed in wandering third instar larvae of *repo>αPS2-RNAi>αPS3-RNAi* and *repo>talin-RNAi*. Boxed regions are magnified in the respective prime panels.

Development (2014) 141, 3072-3083 doi:10.1242/dev.101972

Table 1. Summary of neuronal phenotypes

Genotype	Axonal phenotype class (%)				Total number
	Normal	Mistargeting	Stalling in OS	Stalling in ED	
repo-GAL4	97	3	0	0	60
repo>βPS-RNAi(R1)	30	29	33	8	138
repo>talin-RNAi(GD)	13	28	40	19	103
repo>talin-RNAi(R1)	17	36	36	12	473
**repo-GAL4*	100	0	0	0	40
**repo>βPS-RNAi(GD)*	57	10	11	22	148
**repo>βPS-RNAi(GD)>βPS, αPS2*	98	0	0	2	63
repo>talin-RNAi(GD)>βPS, αPS2	15	4	78	4	27
repo>αPS2-RNAi(GD)	98	2	0	0	52
repo>αPS3-RNAi(R1)	97	3	0	0	39
repo>αPS2-RNAi(GD)>αPS3-RNAi(R1)	82	10	3	5	39
repo>αPS2-RNAi(R1)>αPS3-RNAi(GD)	25	10	25	40	20
tub-GAl80ts, repo-GAL4	99	1	0	0	78
tub-GAl80ts, repo>NrxIV-RNAi(8353)	100	0	0	0	50
tub-GAl80ts, repo>NrxIV-RNAi(9039)	100	0	0	0	62
tub-GAl80ts, repo>βPS-RNAi(R1)	79	7	3	11	116
tub-GAl80ts, repo>βPS-RNAi(R1)>NrxIV-RNAi(8353)	60	10	6	25	122
tub-GAl80ts, repo>βPS-RNAi(R1)>NrxIV-RNAi(9039)	45	10	2	42	162

The genotypes examined for optic stalk morphology changes and photoreceptor axon outgrowth and targeting phenotypes are listed. All RNAi and control crosses were performed with co-expression of UAS-CD8-GFP and at 25°C unless otherwise specified. UAS-Dicer2 was co-expressed in all crosses except those marked with an asterisk. Crosses with tub-GAL80ts (the bottom six genotypes) were conducted using a temperature shift protocol (see Materials and Methods). ED, eye disc; OS, optic stalk.

axons and the ECM rather than forming a monolayer (Fig. 3K,L). We also observed breaks between the glial layers (Fig. 3L).

Loss of βPS integrin and talin in glia causes axonal migration defects

To further address how neurons responded to the glial morphology changes, we used the anti-Chaoptin antibody (mAb 24B10) to label photoreceptor axons. In control larvae, photoreceptor axons pass through the OS to targets in the optic lobe (Fig. 4A-B). Depletion of βPS or talin in the glia resulted in three categories of photoreceptor axon phenotype: (1) mistargeting in the brain; (2) stalling in the OS; and (3) stalling in the ED (Fig. 4C-E, Table 1). These phenotypes were not observed when GMR-GAL4 was used to deplete integrin in the photoreceptor cells (data not shown). Co-expressing a βPS transgene with the βPS-RNAi in glia rescued the axon phenotypes, suggesting that this effect was specific to the knockdown of glial integrin complexes (Fig. 2G, Table 1). The same transgene did not rescue the axon defects observed with talin-RNAi, indicating that rescue was not simply due to attenuation of GAL4 (Table 1). These results suggest that loss of the focal adhesion complex in the OS glia leads to photoreceptor axon defects.

In the mistargeting category, all or most photoreceptor axons successfully passed through the OS but failed to terminate correctly in the optic lobe, forming highly disorganized axon patterns (Fig. 4C,C′). These data suggest that reduced βPS or talin in the glia strongly affects photoreceptor axon guidance in the brain. In the stalling categories, photoreceptor axons either failed to exit the ED (Fig. 4D,D′,F,F′,G,G′) or the OS (Fig. 4E,E′,H,H′). Defects in axonal targeting and lack of photoreceptor innervation were also observed in adult optic lobes (supplementary material Fig. S4), suggesting that these neuronal defects were not corrected at later developmental stages.

The distribution of βPS in glia of the OS led us to test the contribution of each layer in mediating the glia and neuronal phenotypes. However, when drivers specific for each glial layer (C527-GAL4 for PG; SPG-GAL4 for CG; MZ97-GAL4 and Gli-GAL4 for WG) were used to express either βPS or talin-RNAi, none generated the glial or neuronal phenotypes observed using repo-GAL4 (data not shown). These results suggest that these other glial drivers do not generate an effective reduction in βPS, or that the disruption of the integrin complexes in multiple glial layers contributed to the phenotypes observed.

We next analyzed somatic MARCM clones of a null mutation in the *βPS* gene (*mys*^{1}). Previously, we had successfully used the MARCM system to obtain somatic clones of *mys*^{1} in the PG of the peripheral nerve (Xie and Auld, 2011). Using this approach in the optic nerve, we obtained multiple *mys*^{1} clones in the WG, some clones in the PG and occasional clones in one of the two CG (never both). The *mys*^{1} clones observed in the glia of the OS and eye were generally limited in size, and we were unable to obtain clones simultaneously involving both CG and PG cell types. We did not observe the glia or neuronal phenotypes seen with global depletion of βPS with RNAi, suggesting that the loss of βPS or talin in multiple glial layers is necessary for the observed phenotypes. In support of this, when we depleted either αPS2 or αPS3 in all glia using repo-GAL4-driven RNAi, we rarely observed axonal phenotypes (Table 1). However, when we simultaneously depleted αPS2 and αPS3 in all glia, we observed axon stalling phenotypes similar to those of βPS- and talin-RNAi (Fig. 4F,F′, Table 1). As αPS2 and αPS3 are differentially localized to the interface of different glia layers (Fig. 1), these results suggest that the observed axonal phenotypes were due to the combined loss of integrin complexes from multiple glial layers.

Disrupted glial morphology and distribution in the OS are correlated to axon stalling

To further characterize the axon stalling phenotype, F-actin in the axons stalled in the OS was labeled with fluorophore-conjugated phalloidin. In contrast to the control (Fig. 5A), strong phalloidin labeling was detected in the stalling region (Fig. 5B), suggesting that the region might include actin-rich growth cones.

To address the relationship between the glial and axon phenotypes, we analyzed the photoreceptor axons in conjunction with the OS glia. When photoreceptor axons stalled in the OS, clusters of glia aggregated to form a cap-like structure adjacent to

Development (2014) 141, 3072-3083 doi:10.1242/dev.101972

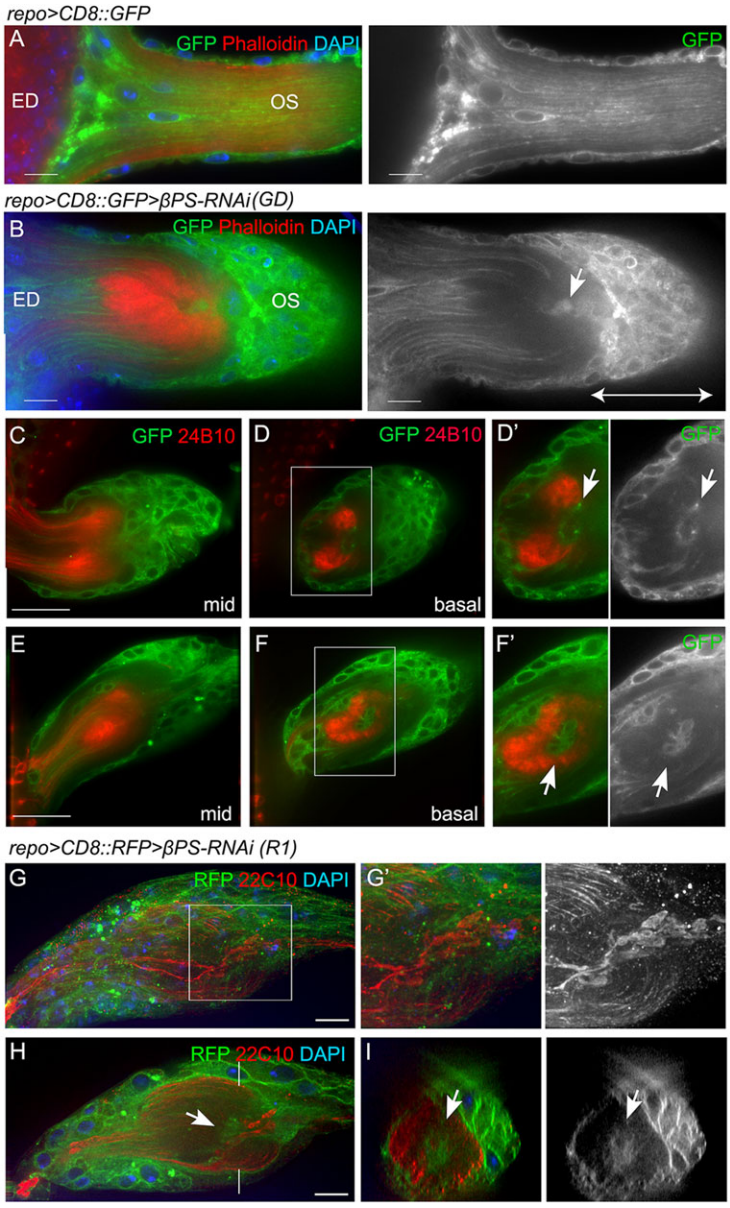

Fig. 5. Axon stalling within the OS. (A,B) Alexa 568-phalloidin (red) was used to label F-actin in control (A) and *repo>βPS-RNAi* (B) ED and OS. Glial membranes were labeled with CD8::GFP (green) and nuclei are marked with DAPI (blue). A glial cap (double-ended arrow) formed proximal to the stalling region, with glia (arrow) present in the stalling region. (C-F′) Glia are associated with stalled axonal terminals. Single optical sections from the middle of the *z*-stack (mid) or from the basal level are shown. Digital magnifications of boxed regions are displayed to the right in grayscale to illustrate the glial membranes. Arrows point to the glia associated with the stalled axon terminals. (G-I) Immunolabeling for Futsch (mAb 22C10, red) marks microtubules in the photoreceptor axons in repo>βPS-RNAi-treated OSs. A projection of the entire stack (G) with the area of axon stalling (G′) are shown. A single optical section from the middle of the stack (H) and the orthogonal sections (I) highlight the stalling region and the glia within it (arrows). All panels except G are single 0.2 μm *z*-sections. Scale bars: 10 μm.

the stall and proximal to the optic lobe (Fig. 5B-F). These glia were closely associated with the stalled axonal terminals (Fig. 5G,H). Glia were observed within the core of the OS surrounded by the stalled photoreceptor axons (Fig. 5D,F,H,I), which frequently segregated into two bundles (Fig. 5C). Occasionally, only one of the two bundles of axons stalled in the RNAi OS (supplementary material Fig. S5) while the other continued into the optic lobe. We observed expanded areas of the microtubule-associated protein Futsch, when immunolabeled (mAb 22C10), associated with the axons within the stalled regions (Fig. 5G-I). These areas were associated with the presence of glia within the OS.

To identify the type of glia associated with the stalled photoreceptor axons, we examined molecular markers for the OS glial subtypes in control and *repo>βPS-RNAi* or *repo>talin-RNAi* larvae. The transcription factor *apontic* (*apt*) is expressed in the PG but not other glial subtypes (Dr C. Klämbt, personal communication). In control OS (n=7), Apt immunolabeling was detected in the peripheral PG nuclei, while the internal WG nuclei were labeled by Gli-lacZ (Fig. 6A). In *repo>βPS-RNAi* most PG and WG nuclei still differentially expressed Apt and Gli-lacZ (Fig. 6B,C). However, we observed a class of glia in the *repo>βPS-RNAi* OSs not labeled by either Apt or Gli-lacZ (n=15 out of 16) (Fig. 6) and a smaller population of glia positive for both Apt and Gli-lacZ (n=8 out of 16) (Fig. 6). The loss or mix of the PG and WG markers in βPS-RNAi OS suggests that the integrin complex might be important for PG/WG differentiation or maintenance of their identities.

Laminin is expressed by the PG in the peripheral nerve (Xie and Auld, 2011) and was tested as another potential PG marker in the OS. In controls, γ-Laminin (LanB2) immunolabeling plus Perlecan (Trol – FlyBase) endogenously tagged with GFP were observed in the ECM ensheathing the OS (Fig. 7A,A′). LanB2 labeling but not Perlecan::GFP was detected in the cytoplasm of the PG, suggesting that the OS PG, like the peripheral nerve PG, are in part responsible for ECM production. In βPS- and talin-depleted OSs, we observed LanB2-positive glia in the core of the OS (Fig. 7B,B′). The LanB2-positive glia were unlikely to be WG as they did not express Gli-lacZ (Fig. 7D-F). We consistently observed mislocalized WG (Gli-lacZ positive, Apt/LanB2 negative) in the glial cap (Fig. 6B,C and Fig. 7E), suggesting that the WG maintained Gli-lacZ expression even when they migrated beyond the stalled axons.

Development (2014) 141, 3072-3083 doi:10.1242/dev.101972

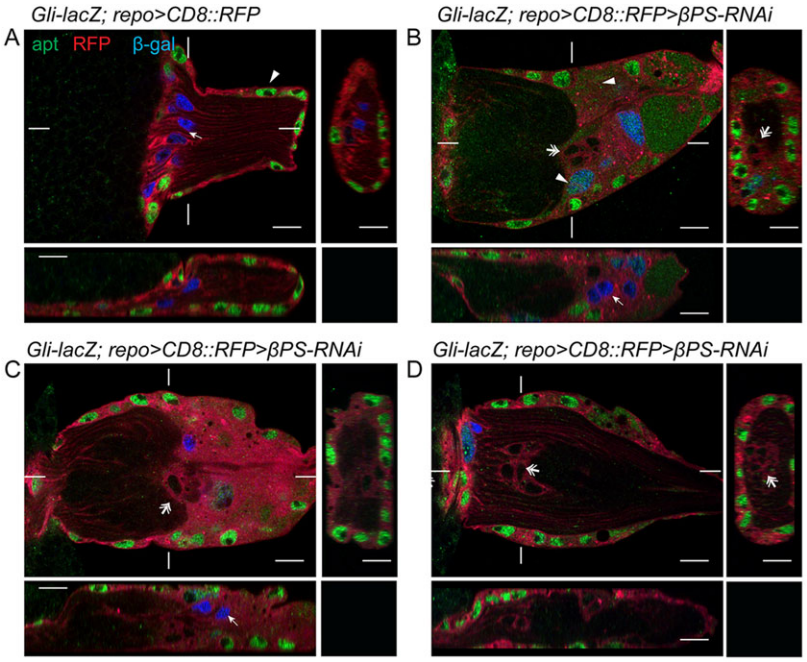

Fig. 6. The glial subtype markers Apontic and Gli-lacZ are altered after focal adhesion loss. An antibody to the transcription factor Apontic (Apt, green) and Gli-lacZ (blue) labeled PG and WG nuclei, respectively. Glial membranes were labeled using repo>CD8::RFP (red). Orthogonal sections were made from the marked positions. (A) In controls (*Gli-lacZ; repo>CD8::RFP*), Apt immunolabeling was detected in all peripheral PG nuclei (arrowhead) and β-galactosidase immunolabeling was restricted to WG nuclei (arrow). (B-D) In *Gli-lacZ; repo>βPS-RNAi* most PG and WG nuclei were differentially labeled by either Apt or Gli-lacZ. However, some glia expressed both markers (arrowheads) or expressed neither (double arrows). Note that some Gli-lacZ-positive WG nuclei (arrows) were observed beyond axonal stalling regions in B and C.

The internal LanB2-positive and Gli-lacZ-negative glia were not observed in controls (n=12) but were observed in the majority of talin-RNAi and βPS-RNAi OSs (86%, n=42). All OSs with stalled axons contained a glial cap that included LanB2-positive glia (n=49). Of those RNAi-treated OSs that did not exhibit stalling (n=22), none contained a glial cap but 27% had at least one internal LanB2-positive glial cell. This suggested a correlation between the presence of ectopic glia, the formation of the glial cap and axonal stalling.

Our finding that CG morphology was disrupted after knockdown of either βPS or talin led to the hypothesis that the ectopic glia might arise from PG that anomalously entered into the OS core due to disruption of the CG tube. To test whether disruption of the CG contributes to the axon stalling phenotypes that we observed, we used repo-GAL4 to express NrxIV-RNAi and temperature-sensitive GAL80 to temporally control expression and bypass embryonic lethality. Expression of NrxIV-RNAi, starting in the second instar stage, disrupted the blood-nerve barrier and resulted in the loss of NrxIV::GFP but did not affect photoreceptor morphology and there was no evidence of axon stalling (Table 1). However, when NrxIV-RNAi was combined with βPS-RNAi, the axon stalling phenotypes were enhanced compared with βPS-RNAi alone (Table 1). These data suggest that the axon stalling phenotypes result from a combination of disruption of the CG and the reduction in glia migration leading to an accumulation of PG in the distal end of the OS.

DISCUSSION

We found that OS glia express integrin complexes that play a role in the development of the glia and axons of the ED and OS. βPS integrin is located in puncta at the glial membrane and associates with talin and ILK. These focal adhesion markers are found between the PG and ECM, plus at the interfaces of the PG-CG and CG-CG layers. We found a different distribution for the αPS2 and αPS3 integrins, which were concentrated at the periphery and interior of the OS, respectively. Our results from RNAi-mediated knockdown revealed that these complexes play important roles in OS glial development, as knockdown led to disruption of PG and CG morphology. Specifically, the loss of βPS integrin or talin caused PG to aggregate in the distal half of the OS, resulting in an accumulation of glia in the OS. The PG formed clusters instead of a surrounding monolayer, suggesting that PG make integrin-mediated associations that maintain their distribution.

The PG migrate between the CG and the basal ECM (Silies et al., 2007), and loss of focal adhesions led to a disruption in PG migration, suggesting that integrin complexes on one or both surfaces play a role in mediating glia migration. The αPS2/βPS heterodimer binds ligands containing the tripeptide RGD sequence (Bunch et al., 1992; Fogerty et al., 1994) and αPS3/βPS binds laminins (Schock and Perrimon, 2003; Stark et al., 1997), so either or both could mediate adhesion of the PG to the ECM. However, it appears that depletion of the integrin complex in apposing glial layers is necessary to disrupt glial migration into the OS, as MARCM clones within the PG alone did not disrupt migration. Integrin function is conserved in mediating glial cell migration either on ECM or neighboring glial surfaces. For example, vertebrate glial studies found that integrins are involved in astrocyte (Milner et al., 1999), oligodendrocyte precursor (Milner et al., 1996) and Schwann cell migration on various ECM molecules (Milner et al., 1997). Loss of β1-integrin in Bergmann glia leads to mislocalization, ectopic migration and disruption of process growth within the vertebrate cerebellum (Frick et al., 2012). ILK and CDC42 within Bergmann glia are required for the β1-integrin-dependent control of process outgrowth (Belvindrah et al., 2006).

Reduction of focal adhesions disrupted the CG sheath and the integrity of the blood-nerve barrier, suggesting that maintenance of the CG tube also requires integrin-mediated adhesion. The disruption of the CG tube is similar to observations made in vertebrates, in which glial tubes are necessary for chain migration of neuroblasts along the rostral migratory stream; β1-integrin plays a role in both chain migration and maintenance of the glial tubes (Belvindrah et al., 2007). However, the link between the integrin complex and the formation or stabilization of the CG tube is currently unknown.

The integrin complex appears to play a limited role in the migration of the WG into the OS. After knockdown of βPS or talin, WG with normal bipolar membrane processes were observed and WG *mys*^{1} MARCM clones had morphologies similar to control

Development (2014) 141, 3072-3083 doi:10.1242/dev.101972

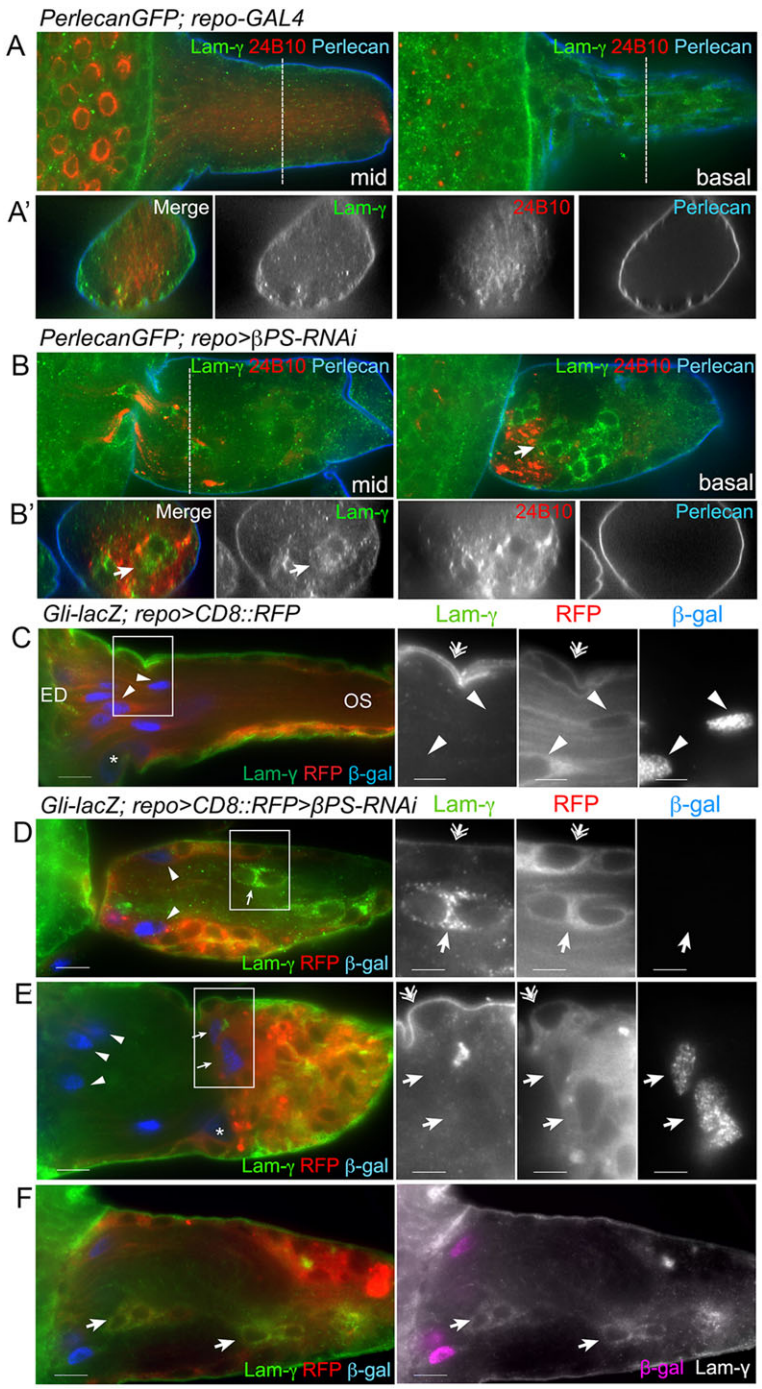

Fig. 7. Ectopic glia express PG markers. (A-B′) LanB2 (Lam-γ, green) and Perlecan::GFP (blue) were used to label the ECM. Photoreceptor neurons were immunolabeled with anti-Chaoptin antibody (mAb 24B10). Two optical sections are shown: midway (mid) and basal. Transverse sections (dashed lines) are shown in the lower panels. In controls (A), both ECM markers were predominantly found in the outermost neural lamella, with only diffuse LanB2 labeling inside the glia. In *repo>βPS-RNAi*, Perlecan::GFP was detected in the neural lamella but glia expressing LanB2 were seen inside the OS associated with stalled axons (arrows). (C-F) LanB2 (green) and Gli-lacZ (β-gal, blue) marked PG and differentiated WG in control (C) and *repo>βPS-RNAi* (D-F) OS. Glial membranes were labeled with *repo>CD8::RFP* (red). Digital magnifications of boxed regions (C-E) are displayed to the right. In controls (C) LanB2 was predominant in the outer ECM and PG (double arrows), but not in the WG, which were distinguished by long membrane processes and Gli-lacZ expression (arrowheads). In *repo>βPS-RNAi* (D-F), LanB2 was detected in the ECM (double arrows) and surface PG. LanB2-positive glia (D,F, arrows) were observed in the OS core along with WG (arrowheads). In some OSs, Gli-lacZ-positive WG were observed in their normal position (E, arrowheads) and in the glial cap proximal to the axonal stalling regions (E, arrows). The majority of OSs had LanB2-positive Gli-lacZ-negative glia within the stalling region and in the glial cap (F, arrows). All panels are single 0.2 μm *z*-sections. Scale bars: 10 μm (left panel); 5 μm (right panels in C-E).

clones (data not shown), suggesting that integrin signaling is not required for migration in differentiated WG. Our TEM analysis suggests that the WG failed to properly ensheath and segregate the bundles of photoreceptor axons, a phenotype consistent with that observed in vertebrate glia, although it is also possible that the lack of WG ensheathment is a secondary effect of axon stalling.

Loss of integrin complexes resulted in a failure of photoreceptor axons to exit the ED, navigate the OS or correctly target the optic lobe. Previously, blocking glial migration from the OS using dominant-negative *Ras1* (*Ras85D* – FlyBase) resulted in photoreceptor axons stalling in the ED but not the OS (Rangarajan et al., 1999). The phenotype suggested that photoreceptor axons require physical contact with retinal glia to exit the ED. However, this mechanism does not seem to apply to the stalling phenotype observed with knockdown of the integrin complex. In the majority of our samples, glia were still present in the ED and around the axonal stalling region, suggesting that the axon stalling phenotypes are likely to be due to a different mechanism.

It is possible that axon stalling results from a combination of glial changes affecting the multiple subtypes of OS glia and disruption of both the βPS/αPS2 and βPS/αPS3 adhesion complexes. Only the simultaneous loss of both αPS2 and αPS3 triggered the axonal phenotypes. Similarly, knockdown of βPS or talin within individual glial subtypes did not trigger axon stalling, whereas disruption of adhesion complexes in all glial subtypes did. It might be that only the repo-GAL4 driver is sufficiently strong or expressed early

Development (2014) 141, 3072-3083 doi:10.1242/dev.101972

enough for the effective knockdown of integrin or talin to trigger the axon stalling phenotypes. However, we can effectively produce the axon stalling phenotype by delaying the expression of the RNAi with the repo-GAL4 driver until the second instar, suggesting that early expression is not key. Overall, our results suggest that it is the combined loss of the focal adhesion complex in multiple glial layers that led to the axon stalling phenotype, although the underlying mechanism is not known. It is possible that the simultaneous aggregation of the stalled PG and disruption of the CG sheath triggers axon stalling by allowing ectopic PG to enter the center of the OS or form the glial cap. The ectopic PG within the axon stalling area and in the glial cap were likely to be PG given their expression of LanB2, Apt and the lack of the WG Gli-lacZ marker. Normally, the PG migrate into the ED and differentiate into WG in the presence of photoreceptor axons. However, in the RNAi-treated OS many of the Apt-positive glia also expressed Gli-lacZ, suggesting a change in the normal differentiation pathway, perhaps owing to the premature and ectopic contact of the PG with the photoreceptors within the OS. Loss of integrins throughout the entire glial population could also lead to global changes to the ECM, as loss of integrins can alter the deposition of ECM components during epithelial morphogenesis (Narasimha and Brown, 2004). Although loss of integrins in the PNS does not lead to changes in the neural lamella of the peripheral nerve (Xie and Auld, 2011), it is possible that ECM changes in terms of structural integrity or the ability to recruit protein components could result in the multiple glial morphological changes.

In summary, we have shown that glia in the OS and ED express integrins and talin, through which they receive external signals important for PG migration, organization and CG barrier formation. The combined impact of integrin complexes on the morphology and development of both glial layers is crucial for proper axonal outgrowth through the OS and targeting in the brain.

MATERIALS AND METHODS

Fly strains and genetics

The following fly strains were used: *repo-GAL4* (Sepp et al., 2001); *spg-GAL4* (Schwabe et al., 2005); *UAS-mCD8::GFP* (Lee and Luo, 1999); *UAS-mCD8::RFP* (a gift from Dr Elizabeth Gavis, Princeton University); *UAS-Dicer2* (Dietzl et al., 2007); *mys*^{1} (Bunch et al., 1992); *FRT19A,tubP-GAL80,hsFLP,w** (Lee and Luo, 1999); *repo-FLP* (Stork et al., 2008); *Gli-lacZ* (Auld et al., 1995); *Perlecan::GFP*; *NrxIV::GFP*; *ILK::GFP; αPS1::YFP* and *αPS2::YFP* (Rees et al., 2011); *talin::GFP* (a gift from Dr Guy Tanentzapf, University of British Columbia). The UAS-RNAi strains used were: *UAS-βPS-RNAi(GD)* (GD15002), *UAS-talin-RNAi(GD)* (GD12050), *UAS-αPS2-RNAi(GD)* (GD44885), *UAS-αPS3-RNAi(GD)* (GD4891), *UAS-NrxIV-RNAi(GD)* (GD2436) (Dietzl et al., 2007); *UAS-βPS-RNAi(R1)* (1560R-1), *UAS-αPS2-RNAi(R1)* (9623R-2), *UAS-αPS3-RNAi(R1)* (8095R-1) and *UAS-talin-RNAi(R1)* (6831R-1) from the National Institute of Genetics, Japan. Unless specified otherwise, RNAi experiments were carried out at 25°C with UAS-Dicer2 plus UAS-mCD8::GFP in control (crossed with w^{1118}) and experimental crosses. UAS-βPS-RNAi(GD) was expressed without Dicer2 as the presence of Dicer2 stalled animal growth in the early third larval instar. GAL80^{ts} was used to control the expression of NrxIV-RNAi and larvae were raised at 18°C until second instar then transferred to 29°C and wandering third instar larvae dissected.

Immunohistochemistry and imaging analysis

The following monoclonal antibodies were obtained from the Developmental Studies Hybridoma Bank (University of Iowa): anti-βPS (CF.6G11) (Brower et al., 1984) at 1:10, anti-αPS2 (CF.2C7) (Brower et al., 1984) at 1:5, anti-Repo (8D12) (Alfonso and Jones, 2002) at 1:50, anti-Chaoptin (24B10) (Fujita et al., 1982) at 1:50, anti-β-galactosidase (40-1a) (Goto and Hayashi, 1999) at 1:50, and anti-Futsch (22C10) at 1:5. Other primary antibodies were: rabbit anti-αPS3 (Wada et al., 2007) at 1:200, rabbit anti-HRP (Jackson ImmunoResearch, 323-005-021) at 1:500, rabbit anti-Laminin-γ (LanB2) (Abcam, ab47651) at 1:100, rabbit anti-talin at 1:500 (a gift from Nicholas Brown, University of Cambridge), and rat anti-Apontic at 1:100 (a gift from Paul MacDonald, University of Texas). All secondary antibodies were used at 1:200 dilution: goat anti-mouse Alexa 568 and 647, goat anti-rabbit Alexa 488, 568 and 647 (Molecular Probes/Invitrogen); peroxidase-conjugated goat anti-mouse IgG (Jackson ImmunoResearch).

Dissection and fixation for immunofluorescence were performed according to standard procedures (Sepp et al., 2000). For βPS integrin immunolabeling, larvae were fixed in 4% paraformaldehyde (PFA) for 10 min. For immunohistochemistry, EDs were incubated with DAB (Sigma-Aldrich) for 30-60 min. For actin staining, eye-brain complexes were incubated with Alexa 568-phalloidin (Molecular Probes) at 1:50.

Fluorescent images were obtained with a DeltaVision microscope (Applied Precision) using a 60× oil immersion objective (NA 1.4) at 0.2 µm steps. Stacks were deconvolved (SoftWorx) using a point spread function (PSF) measured from 0.2 µm fluorescent beads (Molecular Probes) in Vectashield (Vector Laboratories). Fig. 2G and Fig. 6 images were acquired using a Zeiss LSM 700 confocal microscope with a 63× lens (NA 1.4). Images were compiled using ImageJ (NIH), Photoshop (Adobe) and Illustrator CS4 (Adobe). Lower magnification images were taken using a 20× objective (NA 0.4) or a 40× objective (NA 0.75) on an Axioskop2 (Zeiss). DIC images were taken on an Axioskop2 using 5× (NA 0.13) or 20× (NA 0.5) objectives.

For statistical analysis, each replicate (n) represented the glia counted per ED/OS. The average glia number was expressed as mean±s.d. using Prism 6 (GraphPad Software). All comparisons were conducted with a Kruskal–Wallis test with Dunn's multiple comparison post-test. Significant differences were assessed at a 95% confidence interval.

For transmission electron microscopy (TEM) analysis larval brains were fixed in 4% PFA and 3% glutaraldehyde, rinsed in 0.1 M PIPES, post-fixed in 1% osmium tetroxide, embedded in 1:1 acetonitrile:Spurr resin and polymerized in Spurr resin. Thin sections (50 nm) were obtained with a Leica ultramicrotome and analyzed with a FEI Tecnai TEM operating at an accelerating voltage of 80 kV.

Dye permeation assay

Live everted larvae were prepared as described previously (Brink et al., 2012). Individual larva were mounted for imaging in 0.7 mg/ml 10 kDa dextran conjugated with Alexa 647 (Invitrogen/Molecular Probes) dissolved in HL-6 (Macleod et al. 2002), 2 mM Ca^{2+} and 5 mM glutamate. Peripheral nerves and OSs were imaged 10 min and 20 min, respectively, after mounting. Image stacks were collected with a DeltaVision Spectris microscope using a 60× water immersion lens (NA 1.2) and deconvolved with a measured PSF (0.2 µm fluorescent beads in HL-6 plus Ca^{2+} and glutamate). Average pixel intensities of matching interior and exterior areas of each nerve/OS were measured with ImageJ. The ratios of interior versus exterior intensities were analyzed and compared with control using an unpaired t-test with Welch's correction and plotted using Prism 6. The ratio for each genotype was expressed as mean±s.d.

Acknowledgements

We thank Dr Shigeo Hayashi, Dr Nicholas Brown and Dr Paul MacDonald for generously providing antibodies; Dr Cath Cowen for TEM assistance; Drs Guy Tanentzapf, Christian Klämbt, Elizabeth Gavis, Douglas Allan, the Bloomington and DGRC Stock Centers for fly stocks; the TRiP at Harvard Medical School [NIH/NIGMS R01-GM084947] for providing transgenic RNAi fly stocks; and Dr Tim O'Connor for helpful discussions and comments on the manuscript. X.X. and L.P.-R. were supported by scholarships from the Multiple Sclerosis Society of Canada.

Competing interests

The authors declare no competing financial interests.

Author contributions

X.X. contributed to all aspects of the work including writing and editing of the manuscript, study design, data collection, analysis and interpretation. M.G. performed experiments, contributed to data collection, interpretation and editing

of the manuscript. L.P.-R. performed experiments and data collection. V.J.A. contributed study conception and design, data interpretation, writing and editing of the manuscript.

Funding
This study was supported by grants to V.J.A. from the Canadian Institutes of Health Research [MOP-123420] and the Natural Science and Engineering Research Council of Canada [RGPIN 227814-06].

Supplementary material
Supplementary material available online at
http://dev.biologists.org/lookup/suppl/doi:10.1242/dev.101972/-/DC1

References

Alfonso, T. B. and Jones, B. W. (2002). gcm2 promotes glial cell differentiation and is required with glial cells missing for macrophage development in Drosophila. *Dev. Biol.* **248**, 369-383.
Auld, V. J., Fetter, R. D., Broadie, K. and Goodman, C. S. (1995). Gliotactin, a novel transmembrane protein on peripheral glia, is required to form the blood-nerve barrier in Drosophila. *Cell* **81**, 757-767.
Barros, C. S., Nguyen, T., Spencer, K. S. R., Nishiyama, A., Colognato, H. and Muller, U. (2009). β1 integrins are required for normal CNS myelination and promote AKT-dependent myelin outgrowth. *Development* **136**, 2717-2724.
Baumgartner, S., Littleton, J. T., Broadie, K., Bhat, M. A., Harbecke, R., Lengyel, J. A., Chiquet-Ehrismann, R., Prokop, A. and Bellen, H. J. (1996). A Drosophila neurexin is required for septate junction and blood-nerve barrier formation and function. *Cell* **87**, 1059-1068.
Belvindrah, R., Nalbant, P., Ding, S., Wu, C., Bokoch, G. M. and Müller, U. (2006). Integrin-linked kinase regulates Bergmann glial differentiation during cerebellar development. *Mol. Cell. Neurosci.* **33**, 109-125.
Belvindrah, R., Hankel, S., Walker, J., Patton, B. L. and Muller, U. (2007). β1 integrins control the formation of cell chains in the adult rostral migratory stream. *J. Neurosci.* **27**, 2704-2717.
Benninger, Y., Thurnherr, T., Pereira, J. A., Krause, S., Wu, X., Chrostek-Grashoff, A., Herzog, D., Nave, K.-A., Franklin, R. J. M., Meijer, D. et al. (2007). Essential and distinct roles for cdc42 and rac1 in the regulation of Schwann cell biology during peripheral nervous system development. *J. Cell Biol.* **177**, 1051-1061.
Brakebusch, C. and Fässler, R. (2003). The integrin-actin connection, an eternal love affair. *EMBO J.* **22**, 2324-2333.
Brink, D. L., Gilbert, M., Xie, X., Petley-Ragan, L. and Auld, V. J. (2012). Glial processes at the Drosophila larval neuromuscular junction match synaptic growth. *PLoS ONE* **7**, e37876.
Brower, D. L., Wilcox, M., Piovant, M., Smith, R. J. and Reger, L. A. (1984). Related cell-surface antigens expressed with positional specificity in Drosophila imaginal discs. *Proc. Natl. Acad. Sci. USA* **81**, 7485-7489.
Brown, N. H., Gregory, S. L. and Martin-Bermudo, M. D. (2000). Integrins as mediators of morphogenesis in Drosophila. *Dev. Biol.* **223**, 1-16.
Bunch, T. A., Salatino, R., Engelsgjerd, M. C., Mukai, L., West, R. F. and Brower, D. L. (1992). Characterization of mutant alleles of myospheroid, the gene encoding the beta subunit of the Drosophila PS integrins. *Genetics* **132**, 519-528.
Camara, J., Wang, Z., Nunes-Fonseca, C., Friedman, H. C., Grove, M., Sherman, D. L., Komiyama, N. H., Grant, S. G., Brophy, P. J., Peterson, A. et al. (2009). Integrin-mediated axoglial interactions initiate myelination in the central nervous system. *J. Cell Biol.* **185**, 699-712.
Clegg, D. O., Wingerd, K. L., Hikita, S. T. and Tolhurst, E. C. (2003). Integrins in the development, function and dysfunction of the nervous system. *Front. Biosci.* **8**, d723-d750.
Critchley, D. R. (2000). Focal adhesions - the cytoskeletal connection. *Curr. Opin. Cell Biol.* **12**, 133-139.
Critchley, D. R., Holt, M. R., Barry, S. T., Priddle, H., Hemmings, L. and Norman, J. (1999). Integrin-mediated cell adhesion: the cytoskeletal connection. *Biochem. Soc. Symp.* **65**, 79-99.
Dietzl, G., Chen, D., Schnorrer, F., Su, K.-C., Barinova, Y., Fellner, M., Gasser, B., Kinsey, K., Oppel, S., Scheiblauer, S. et al. (2007). A genome-wide transgenic RNAi library for conditional gene inactivation in Drosophila. *Nature* **448**, 151-156.
Eroglu, C. and Barres, B. A. (2010). Regulation of synaptic connectivity by glia. *Nature* **468**, 223-231.
Feltri, M. L., Graus Porta, D., Previtali, S. C., Nodari, A., Migliavacca, B., Cassetti, A., Littlewood-Evans, A., Reichardt, L. F., Messing, A., Quattrini, A. et al. (2002). Conditional disruption of beta1 integrin in Schwann cells impedes interactions with axons. *J. Cell Biol.* **156**, 199-219.
Fogerty, F. J., Fessler, L. I., Bunch, T. A., Yaron, Y., Parker, C. G., Nelson, R. E., Brower, D. L., Gullberg, D. and Fessler, J. H. (1994). Tiggrin, a novel Drosophila extracellular matrix protein that functions as a ligand for Drosophila alpha PS2 beta PS integrins. *Development* **120**, 1747-1758.
Franzdottir, S. R., Engelen, D., Yuva-Aydemir, Y., Schmidt, I., Aho, A. and Klambt, C. (2009). Switch in FGF signalling initiates glial differentiation in the Drosophila eye. *Nature* **460**, 758-761.
Freeman, M. R. and Doherty, J. (2006). Glial cell biology in Drosophila and vertebrates. *Trends Neurosci.* **29**, 82-90.
Frick, A., Grammel, D., Schmidt, F., Pöschl, J., Priller, M., Pagella, P., von Bueren, A. O., Peraud, A., Tonn, J. C., Herms, J. et al. (2012). Proper cerebellar development requires expression of β1-integrin in Bergmann glia, but not in granule neurons. *Glia* **60**, 820-832.
Fujita, S. C., Zipursky, S. L., Benzer, S., Ferrus, A. and Shotwell, S. L. (1982). Monoclonal antibodies against the Drosophila nervous system. *Proc. Natl. Acad. Sci. USA* **79**, 7929-7933.
Goto, S. and Hayashi, S. (1999). Proximal to distal cell communication in the Drosophila leg provides a basis for an intercalary mechanism of limb patterning. *Development* **126**, 3407-3413.
Grove, M., Komiyama, N. H., Nave, K.-A., Grant, S. G., Sherman, D. L. and Brophy, P. J. (2007). FAK is required for axonal sorting by Schwann cells. *J. Cell Biol.* **176**, 277-282.
Han, C., Wang, D., Soba, P., Zhu, S., Lin, X., Jan, L. Y. and Jan, Y.-N. (2012). Integrins regulate repulsion-mediated dendritic patterning of drosophila sensory neurons by restricting dendrites in a 2D space. *Neuron* **73**, 64-78.
Lee, T. and Luo, L. (1999). Mosaic analysis with a repressible cell marker for studies of gene function in neuronal morphogenesis. *Neuron* **22**, 451-461.
Lee, K. K., De Repentigny, Y., Saulnier, R., Rippstein, P., Macklin, W. B. and Kothary, R. (2006). Dominant-negative β1 integrin mice have region-specific myelin defects accompanied by alterations in MAPK activity. *Glia* **53**, 836-844.
Macleod, G. T., Hegstrom-Wojtowicz, M., Charlton, M. P. and Atwood, H. L. (2002). Fast calcium signals in Drosophila motor neuron terminals. *J. Neurophysiol.* **88**, 2659-2663.
Milner, R. and Campbell, I. L. (2002). The integrin family of cell adhesion molecules has multiple functions within the CNS. *J. Neurosci. Res.* **69**, 286-291.
Milner, R., Edwards, G., Streuli, C. and Ffrench-Constant, C. (1996). A role in migration for the alpha V beta 1 integrin expressed on oligodendrocyte precursors. *J. Neurosci.* **16**, 7240-7252.
Milner, R., Wilby, M., Nishimura, S., Boylen, K., Edwards, G., Fawcett, J., Streuli, C., Pytela, R. and ffrench-Constant, C. (1997). Division of labor of Schwann cell integrins during migration on peripheral nerve extracellular matrix ligands. *Dev. Biol.* **185**, 215-228.
Milner, R., Huang, X., Wu, J., Nishimura, S., Pytela, R., Sheppard, D. and ffrench-Constant, C. (1999). Distinct roles for astrocyte alphavbeta5 and alphavbeta8 integrins in adhesion and migration. *J. Cell Sci.* **112**, 4271-4279.
Murakami, S., Umetsu, D., Maeyama, Y., Sato, M., Yoshida, S. and Tabata, T. (2007). Focal adhesion kinase controls morphogenesis of the Drosophila optic stalk. *Development* **134**, 1539-1548.
Narasimha, M. and Brown, N. H. (2004). Novel functions for integrins in epithelial morphogenesis. *Curr. Biol.* **14**, 381-385.
Newbern, J. and Birchmeier, C. (2010). Nrg1/ErbB signaling networks in Schwann cell development and myelination. *Semin. Cell Dev. Biol.* **21**, 922-928.
Nodari, A., Zambroni, D., Quattrini, A., Court, F. A., D'Urso, A., Recchia, A., Tybulewicz, V. L. J., Wrabetz, L. and Feltri, M. L. (2007). β1 integrin activates Rac1 in Schwann cells to generate radial lamellae during axonal sorting and myelination. *J. Cell Biol.* **177**, 1063-1075.
Parker, R. J. and Auld, V. J. (2006). Roles of glia in the Drosophila nervous system. *Semin. Cell Dev. Biol.* **17**, 66-77.
Pereira, J. A., Benninger, Y., Baumann, R., Goncalves, A. F., Ozcelik, M., Thurnherr, T., Tricaud, N., Meijer, D., Fassler, R., Suter, U. et al. (2009). Integrin-linked kinase is required for radial sorting of axons and Schwann cell remyelination in the peripheral nervous system. *J. Cell Biol.* **185**, 147-161.
Perkins, A. D., Ellis, S. J., Asghari, P., Shamsian, A., Moore, E. D. W. and Tanentzapf, G. (2010). Integrin-mediated adhesion maintains sarcomeric integrity. *Dev. Biol.* **338**, 15-27.
Previtali, S. C., Feltri, M. L., Archelos, J. J., Quattrini, A., Wrabetz, L. and Hartung, H.-P. (2001). Role of integrins in the peripheral nervous system. *Prog. Neurobiol.* **64**, 35-49.
Rangarajan, R., Gong, Q. and Gaul, U. (1999). Migration and function of glia in the developing Drosophila eye. *Development* **126**, 3285-3292.
Rees, J. S., Lowe, N., Armean, I. M., Roote, J., Johnson, G., Drummond, E., Spriggs, H., Ryder, E., Russell, S., St Johnston, D. et al. (2011). In vivo analysis of proteomes and interactomes using Parallel Affinity Capture (iPAC) coupled to mass spectrometry. *Mol. Cell. Proteomics* **10**, M110.002386.
Schock, F. and Perrimon, N. (2003). Retraction of the Drosophila germ band requires cell-matrix interaction. *Genes Dev.* **17**, 597-602.
Schwabe, T., Bainton, R. J., Fetter, R. D., Heberlein, U. and Gaul, U. (2005). GPCR signaling is required for blood-brain barrier formation in drosophila. *Cell* **123**, 133-144.
Sepp, K. J., Schulte, J. and Auld, V. J. (2000). Developmental dynamics of peripheral glia in Drosophila melanogaster. *Glia* **30**, 122-133.
Sepp, K. J., Schulte, J. and Auld, V. J. (2001). Peripheral glia direct axon guidance across the CNS/PNS transition zone. *Dev. Biol.* **238**, 47-63.

Silies, M., Yuva, Y., Engelen, D., Aho, A., Stork, T. and Klambt, C. (2007). Glial cell migration in the eye disc. *J. Neurosci.* **27**, 13130-13139.
Silies, M., Yuva-Aydemir, Y., Franzdottir, S. R. and Klämbt, C. (2010). The eye imaginal disc as a model to study the coordination of neuronal and glial development. *Fly* **4**, 71-79.
Stark, K. A., Yee, G. H., Roote, C. E., Williams, E. L., Zusman, S. and Hynes, R. O. (1997). A novel alpha integrin subunit associates with betaPS and functions in tissue morphogenesis and movement during Drosophila development. *Development* **124**, 4583-4594.
Stork, T., Engelen, D., Krudewig, A., Silies, M., Bainton, R. J. and Klambt, C. (2008). Organization and function of the blood brain barrier in Drosophila. *J. Neurosci.* **28**, 587-597.
Takada, Y., Ye, X. and Simon, S. (2007). The integrins. *Genome Biol.* **8**, 215.
Tayler, T. D. and Garrity, P. A. (2003). Axon targeting in the Drosophila visual system. *Curr. Opin. Neurobiol.* **13**, 90-95.
Wada, A., Kato, K., Uwo, M. F., Yonemura, S. and Hayashi, S. (2007). Specialized extraembryonic cells connect embryonic and extraembryonic epidermis in response to Dpp during dorsal closure in Drosophila. *Dev. Biol.* **301**, 340-349.
Xie, X. and Auld, V. J. (2011). Integrins are necessary for the development and maintenance of the glial layers in the Drosophila peripheral nerve. *Development* **138**, 3813-3822.
Yu, W.-M., Chen, Z.-L., North, A. J. and Strickland, S. (2009). Laminin is required for Schwann cell morphogenesis. *J. Cell Sci.* **122**, 929-936.

Supplemental Data

Supplemental Figure Legends

Figure S1 (related to Figure 1): Focal adhesion complexes in the wandering 3rd instar ED and OS.
Labeling of the focal adhesion complex components in the wandering 3rd instar (wL3) eye disc and OS. All glial membranes were labeled using repo-GAL4>CD8::GFP (A,B: green); repo-GAL4>CD8::RFP (E,F: blue). Neurons were immunolabeled using anti-HRP (A,B: blue) and nuclei using DAPI (C,D: blue). βPS integrin was detected through immunolabeling (A-I; red) and the alpha integrin subunits were labeled using αPS2 endogenously tagged with YFP (αPS2::YFP, C,D: green) and immunolabeling for αPS3 (H,I: blue). Other focal adhesion components were labeled using Talin and Integrin linked kinase (ILK) endogenously tagged with GFP (Talin::GFP, E-G: green)(ILK::GFP, H,I: green).
All panels are single 0.2 μm Z-sections and for all panels single Z sections at the basal side (basal) and through the mid point (mid) are shown. Dashed lines show where the cross sections (B, D, G, I) are obtained. White boxed regions were shown in higher magnification in small panels (F). In all tissues, focal adhesion complexes including integrins, Talin and ILK were seen throughout the OS and ED. Note that the complexes were strongly detected at the basal level of the OS where glia contact the neural lamella. Scale bars are 10 μm.

Figure S2 (related to Figure 2): Knock down of integrin and OS morphological changes in the early 3rd instar.
repo-GAL4 was used to express βPS-RNAi and talin-RNAi in all glia. UAS-CD8::GFP (green) labeled glial membranes and DAPI (blue, A-C) marked nuclei. Images were projections of 0.2 μm Z-stacks. In controls (A and D), βPS (red) and αPS3 (blue, D) immunolabeling was detected as puncta in the eye disc and OS. These puncta were absent in βPS-RNAi treated OS (B) and decreased in talin-RNAi OS (C and E) (arrows), but still present in the eye disc epithelia (double arrows). Similarly immunolabeling for Talin was observed in puncta (F, red) throughout the wild-type OS labeled with NrxIV::GFP (green) and was reduced in the OS (G, arrow) of Talin-RNAi but retained in the ED (G, double arrow) and the photoreceptor axons. Note that the PG were concentrated in the anterior half (close to ED) and reduced in the posterior half (arrowheads) of RNAi OS. Scale bars are 5 microns (A-F) and 10 microns (G).

Figure S3 (related to Figure 3): Dye penetration after βPS, talin and NrxIV knockdown in OS and peripheral nerves.
Dye permeability assays were conducted to determine the degree of blood-nerve-barrier disruption with loss of integrin and talin in the glia. In control animals, Alexa-647 conjugated dextran was excluded from the interior of the peripheral nerve (A) and the OS (E). The penetration of the fluorescent dye significantly increased in the peripheral nerve (B-D) and OS (F-H) when NrxIV-RNAi (positive control), βPS-RNAi or talin-RNAi were expressed in either the subperineurial (SGP-GAL4) or all glia (repo-GAL4). The quantification of the dye penetration into the OS for βPS-, talin- and NrxIV-RNAi is

shown in Figure 3.

Figure S4 (related to Figure 4): Photoreceptor axon targeting defects in RNAi adults.
A monoclonal 24B10 antibody was used to label photoreceptor axon in adult fly eye-brain complexes. In controls (A), 24B10 labeled photoreceptor axons terminated properly in the optic lobe (OL). Note that left panel shows axonal termination in both lamina (La) and medulla (Me) layers and only medulla was preserved in the right panel. In RNAi flies (B,C), different neuronal defects were observed, which included disorganized axons termination (arrowheads) and lack of photoreceptor innervation (B, C) in the optic lobe. Smaller optic lobes were seen associated with the abbreviated axonal termination. Dashed lines show the boundary between the optic lobe and midbrain (MB).

Figure S5 (related to Figure 5): Axon stalling phenotypes
Examples of axonal stalling and associated glia in the OS (C-E) or ED (A,B,B'). The stalling region was shown by single optic sections either from the middle of the Z-stack (mid) or from the basal level (basal). Regions in white boxes are digitally magnified and displayed in the right panels. Arrows point to the glia associated with the stalled axon terminals.
C-E) Partial stalling phenotypes were observed (C,D) and these represented relatively rare cases where only subsets of photoreceptor axons (arrows) were stalled in the RNAi OS while others migrated through. E) An example of axonal stalling (arrow) at the boundary of the ED and OS.
All panels are single 0.2 μm Z-sections. Scale bars are 10 μm.

Figure S1

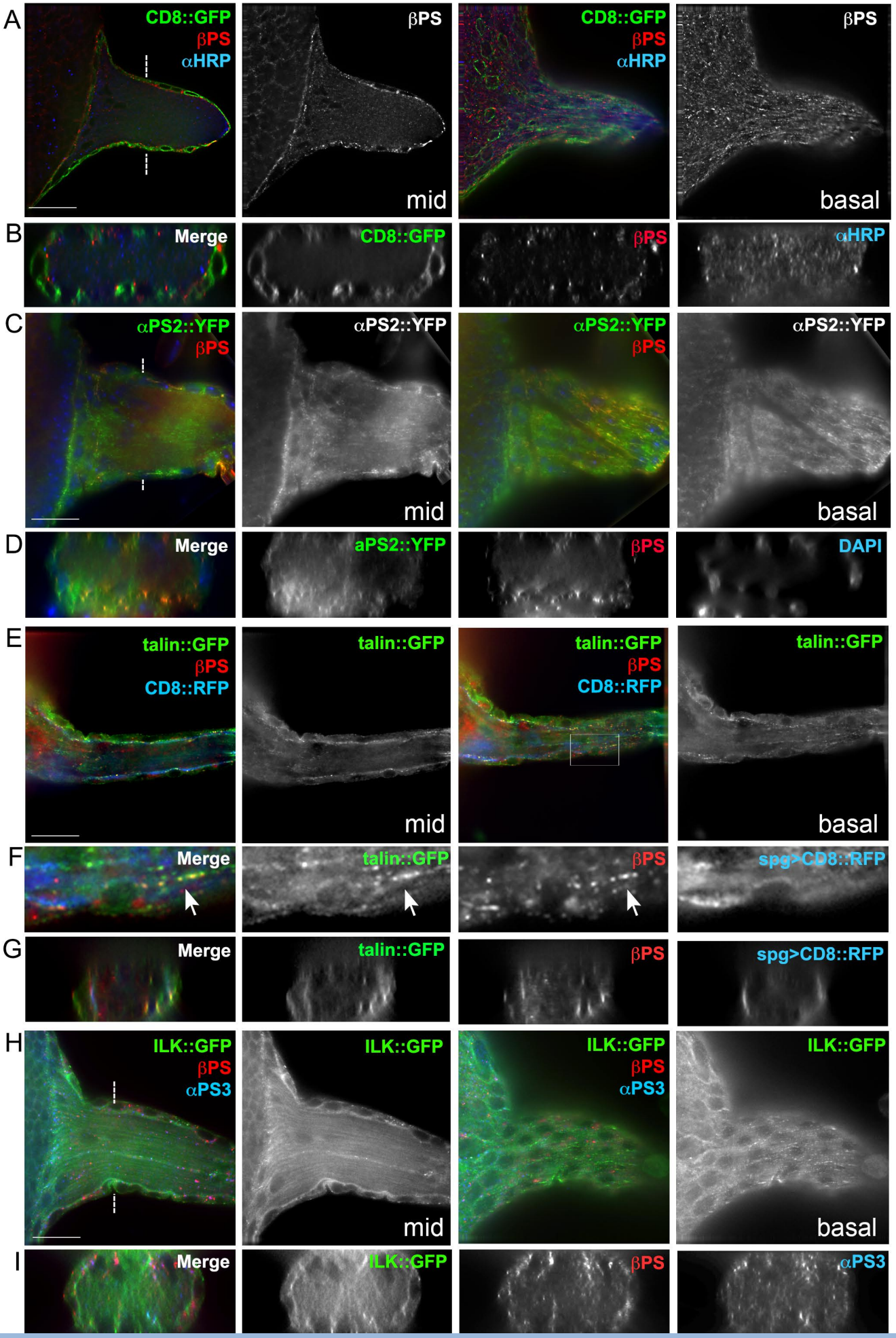
A
CD8::GFP
βPS
αHRP
βPS
mid
CD8::GFP
βPS
αHRP
βPS
basal
B
Merge
CD8::GFP
βPS
αHRP
C
αPS2::YFP
βPS
αPS2::YFP
mid
αPS2::YFP
βPS
αPS2::YFP
basal
D
Merge
aPS2::YFP
βPS
DAPI
E
talin::GFP
βPS
CD8::RFP
talin::GFP
mid
talin::GFP
βPS
CD8::RFP
talin::GFP
basal
F
Merge
talin::GFP
βPS
spg>CD8::RFP
G
Merge
talin::GFP
βPS
spg>CD8::RFP
H
ILK::GFP
βPS
αPS3
ILK::GFP
mid
ILK::GFP
βPS
αPS3
ILK::GFP
basal
I
Merge
ILK::GFP
βPS
αPS3

Figure S2

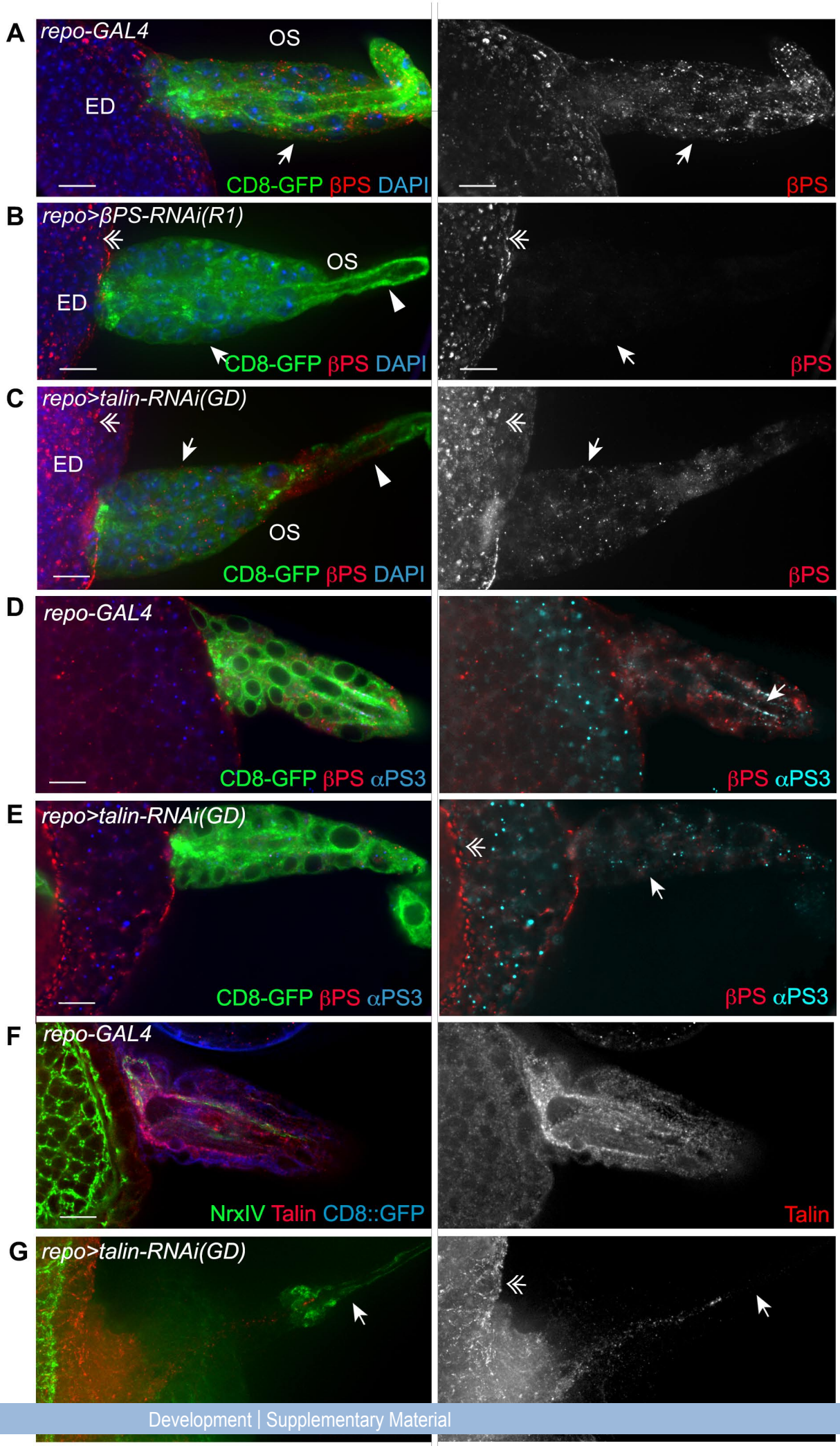
A
repo-GAL4
OS
ED
CD8-GFP βPS DAPI
βPS
B
repo>βPS-RNAi(R1)
OS
ED
CD8-GFP βPS DAPI
βPS
C
repo>talin-RNAi(GD)
ED
OS
CD8-GFP βPS DAPI
βPS
D
repo-GAL4
CD8-GFP βPS αPS3
βPS αPS3
E
repo>talin-RNAi(GD)
CD8-GFP βPS αPS3
βPS αPS3
F
repo-GAL4
NrxIV Talin CD8::GFP
Talin
G
repo>talin-RNAi(GD)

Figure S3

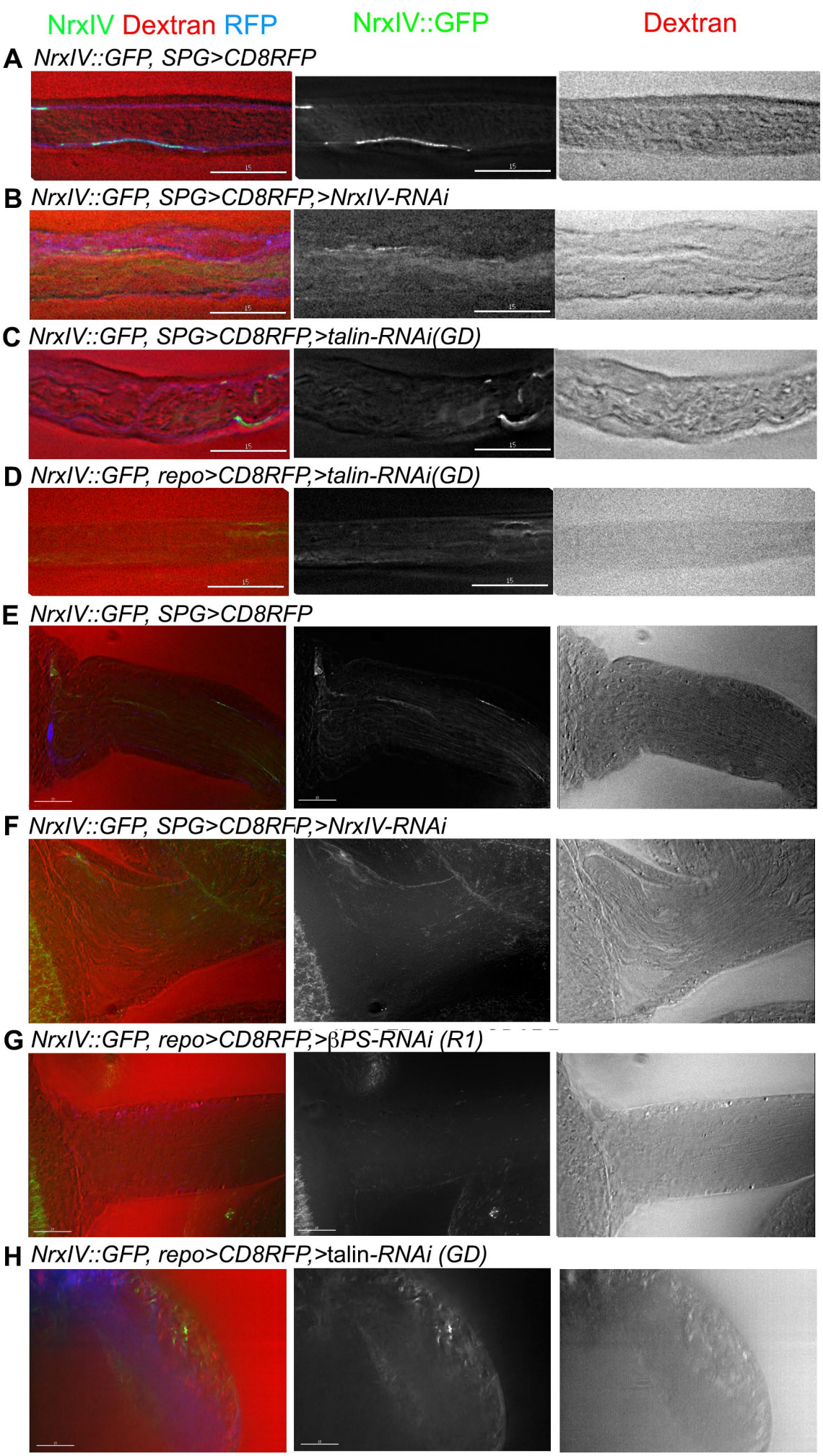
NrxIV Dextran RFP
NrxIV::GFP
Dextran
A NrxIV::GFP, SPG>CD8RFP
B NrxIV::GFP, SPG>CD8RFP,>NrxIV-RNAi
C NrxIV::GFP, SPG>CD8RFP,>talin-RNAi(GD)
D NrxIV::GFP, repo>CD8RFP,>talin-RNAi(GD)
E NrxIV::GFP, SPG>CD8RFP
F NrxIV::GFP, SPG>CD8RFP,>NrxIV-RNAi
G NrxIV::GFP, repo>CD8RFP,>βPS-RNAi (R1)
H NrxIV::GFP, repo>CD8RFP,>talin-RNAi (GD)

Figure S4

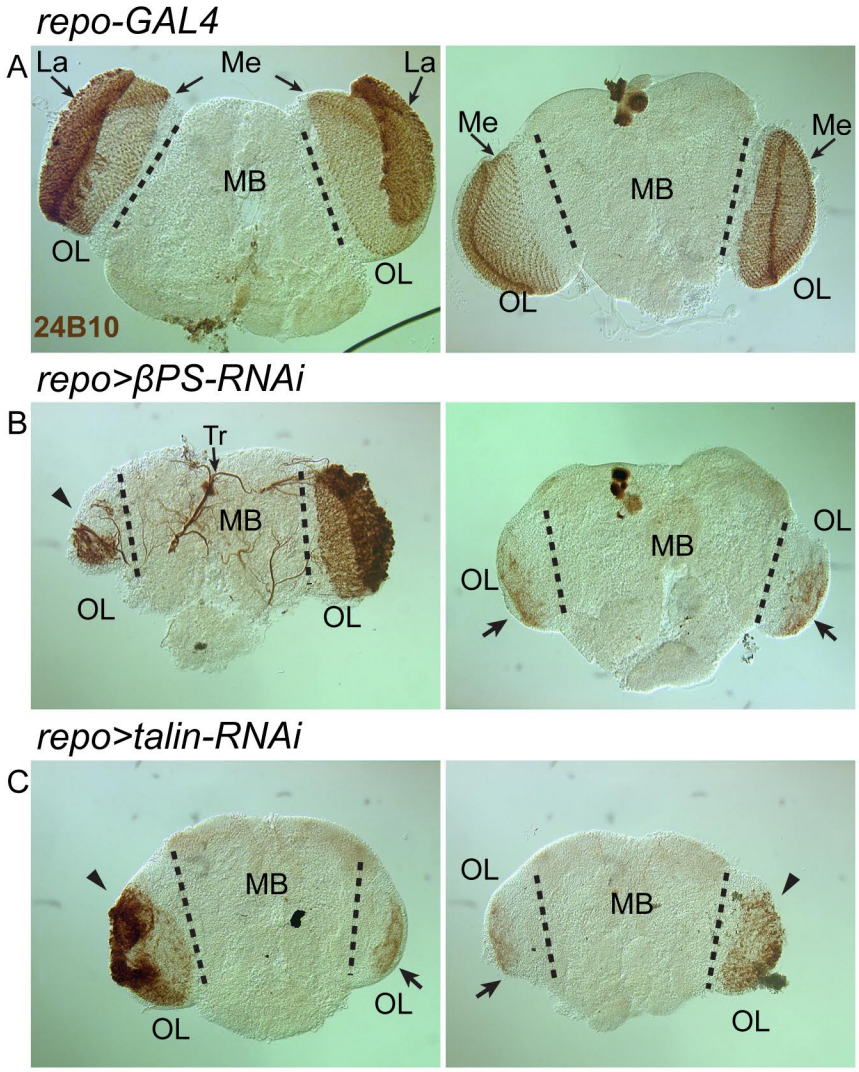
repo-GAL4
A
La
Me
La
MB
OL
OL
24B10
Me
Me
MB
OL
OL
repo>βPS-RNAi
B
Tr
MB
OL
OL
MB
OL
OL
repo>talin-RNAi
C
MB
OL
OL
OL
MB
OL

Figure S5

repo>CD8::GFP>βPS-RNAi (R1)